QIRT'2022

10.21611/qirt.2022.2009

16th Quantitative InfraRed Thermography Conference

Method and test stand for calibrating the thermal imaging camera

by T. Sosnowski*, M. Kastek*, G. Bieszczad*, S. Gogler*, B. Więcek**, R. Strąkowski**, M. Felczak**

* *Military University of Technology, Institute of Optoeletronics, 2 gen.Sylwestra Kaliskiego St. 00-908 Warsaw, Poland*
** *Lodz University of Technology, Institute of Electronics, 211/215 Wólczańska St. 90-924 Łódź, Poland*

Abstract

Thermal imaging cameras are being used in more and more areas of science, technology and life. The result of this is the growing production of thermal imaging cameras that need to be calibrated and their parameters assessed. This paper presents test stands and methods for measuring parameters and calibrating thermal imaging cameras to test and determine the correctness of their operation, as well as to objectively evaluate and compare their parameters.

1. Introduction

Technological development in the field of infrared technology and thermal imaging has resulted in thermal cameras being used not only in such fields as military equipment [1], police, medicine, or in scientific research, but also in many other fields [2] such as automotive, alarm systems, production supervision systems, etc. A thermal imaging camera is a device of considerable complexity, built from such basic elements as [2, 3]: the infrared detector array module, the lens for the infrared range, the electronic circuits that provide the detector signal reading, recording and analysis and the video module. The general scheme of the thermal imaging camera is shown in Figure 1 .

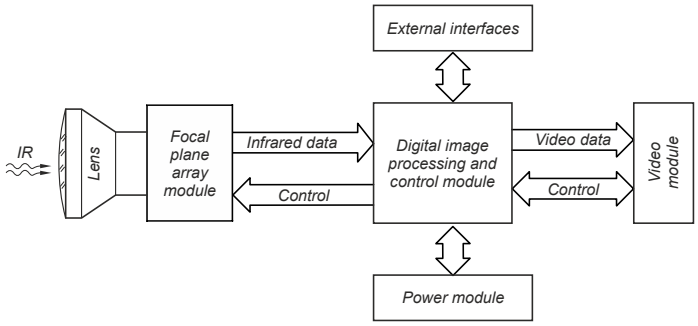

Fig. 1. *General scheme of a thermal imaging camera divided into basic functional modules*

A thermal imaging camera captures infrared radiation from the observed objects via an infrared focal plane array module consisting of a detector array, power and signal conditioning circuits and digital control signal buffers. Uncooled detectors, which can operate at room temperature, are commonly used in thermal imaging cameras. The detectors used in such cameras are usually bolometric detectors belonging to the group of thermal detectors.

Another high-tech thermal imaging camera component is the infrared lens, usually made of germanium or silicon crystal. One of the more complex units of a thermal imaging camera is the control and digital signal processing unit. The control and digital image processing unit is usually built based on a programmable system and a microprocessor system. The programmable system performs image data processing, which requires relatively large computational power, while the microprocessor system performs camera control and other actions characterized by relatively small computational load.

The quality of camera performance is affected by a large number of camera parameters [4, 5, 6, 7]. Therefore, a significant number of physical phenomena such as power source noise, detector array noise, detector temperature, ambient temperature, digital data rate and processing method, and analog-to-digital processing parameters (e.g., quantization noise) must be taken into account when designing a thermal camera. The performance of a thermal imaging camera, especially the one with an uncooled detector array, depends significantly on the environmental parameters. The basic environmental parameters that have the greatest impact on the camera's operation are temperature, electromagnetic interference and atmospheric transmission. In order to determine the quality of the tested thermal imaging camera, it is necessary to measure and determine many parameters of the camera such as sensitivity, non-uniformity, NETD, MRTD and perform non-uniformity correction (NUC). In order to carry out research, testing, objective evaluation and comparison of thermal imaging cameras, it is necessary to have a proper laboratory base to measure and control test parameters and to determine and analyse characteristics and relationships.

2. Thermal imaging camera parameters

Microbolometer detectors of infrared radiation belonging to the group of thermal detectors are commonly used in thermal imaging cameras. Due to the fact that they do not require cryogenic cooling and can operate properly at room temperature they are often called uncooled detectors [8]. Bolometers operate on the principle of change of electrical resistance of the sensor (thermometer) under the influence of temperature change caused by absorption (by the absorber) of incident radiation. The absorber is a thin layer of titanium nitride, which is deposited onto a thermometer usually made of amorphous silicon doped with hydrogen (α-Si:H) [9] or vanadium oxide (VOx) [8]. Based on the change in resistance, the readout integrated circuit (ROIC) generates a voltage signal corresponding to the change in energy of the incident radiation on the detector. Voltage response of the detectors in the array are a subject of analog to digital conversion. Conversion happens for every detector in array in constant time periods yielding a signal that is discreet in space (rows and columns), time (frames) and level (voltage).

The infrared detector array with its associated electronics is subjected to tests of parameters that affect the quality of the thermal image. During such tests and measurements, it is necessary to record measurement data containing K images, each of which has M rows and N columns. The signal read from each detector of the array is recorded in the form of a voltage of value $V(m,n,k,T)$ (signal in the form of a voltage read from the detector located in m – th row and i n -th column in k -th image (frame), which was induced by radiation of an object with temperature T). The basic parameters can be divided into two groups. The first group of parameters describes the properties of a particular array detector. The second group of parameters describes the properties of the entire array of detectors. The following parameters can be distinguished that characterize the properties of a particular detector over time for a fixed irradiance defined by the temperature of the signal (radiation) source:

- The average value for the detector:

$$\overline{V}(m,n,T) = \frac{1}{K}\sum_{k=1}^{K} V(m,n,k,T), \tag{1}$$

- The mean squared value for the detector:

$$\overline{V^2}\,(m,n,T) = \frac{1}{K}\sum_{k=1}^{K} V^2\,(m,n,k,T), \tag{2}$$

- standard deviation for the detector:

$$S\,(m,n,T) = \sqrt{\frac{1}{K-1}\sum_{k=1}^{K}\left[V(m,n,k,T) - \overline{V}(m,n,T)\right]^2}. \tag{3}$$

The parameters defined by the following formulas are used to evaluate the entire detector array:

- The average value for the detector array:

$$\overline{V}_{FPA}(T) = \frac{1}{MN}\sum_{m=1}^{M}\sum_{n=1}^{N} V(m,n,T), \tag{4}$$

- The mean squared value for the detector array:

$$\overline{V^2}_{FPA}(T) = \frac{1}{MN}\sum_{m=1}^{M}\sum_{n=1}^{N} V^2(m,n,T), \tag{5}$$

- standard deviation for the detector array:

$$\overline{S}_{FPA}(T) = \frac{1}{MN}\sum_{m=1}^{M}\sum_{n=1}^{N} S(m,n,T). \tag{6}$$

The sensitivity of a detector array can be determined by measuring the response of the array detectors to an infrared radiation from a surface radiation source having blackbody characteristics at two different temperatures T_1 and T_2. Then the sensitivity of each detector array can be determined using the formula:

$$R(m,n) = \frac{V(m,n,k,T_2) - V(m,n,k,T_1)}{T_2 - T_1} \cdot \frac{1}{\Omega_{norm}(m,n)}. \tag{7}$$

Then, the sensitivity of the entire detector array can be expressed as:

$$R_{FPA} = \frac{1}{N_{VR}} \sum_{m=1}^{M} \sum_{n=1}^{N} R_{VR}\,(m,n), \tag{8}$$

where:

$$R_{VR}\,(m,n) = \begin{cases} R(m,n) & \text{if} \quad R(m,n) \in \left((1-k_{VR})\cdot\overline{R};(1+k_{VR})\cdot\overline{R}\right) \\ 0 & \text{if} \quad R(m,n) \notin \left((1-k_{VR})\cdot\overline{R};(1+k_{VR})\cdot\overline{R}\right) \end{cases} \tag{9}$$

$$\overline{R} = \frac{1}{MN} \sum_{m=1}^{M} \sum_{n=1}^{N} R(m,n), \tag{10}$$

N_{VR} - number of detectors for which the condition $R(m,n) \in \left((1-k_{VR})\cdot\overline{R};(1+k_{VR})\cdot\overline{R}\right)$ is met, k_{VR} - coefficient selected depending on the type of detector and camera construction.

The RMS noise value of a given detector in an array can be determined by calculating the square root of the variance of the signal read for successive moments. It is assumed that the intensity of the radiation incident on the detector remains constant during the measurement. For images discrete in time, the RMS noise value of the detector located in the m-th row and n-th column is given as the square root of the unbiased estimator of variance and is given by the equation:

$$noise(m,n) = \sqrt{\frac{1}{K-1} \sum_{k=1}^{K} \left[V(m,n,k) - \overline{V}(m,n)\right]^2}, \tag{11}$$

where $\overline{V}(m,n)$ is the mean value of the response of the detector located in m-th row and n-th column, given by the formula (1).

In order to quantify the noise for all detectors in the array (detector array noise), a parameter defined as the average noise of the array detectors was introduced, given by the formula:

$$noise_{FPA}(m,n) = \frac{1}{MN} \sum_{m=1}^{M} \sum_{n=1}^{N} noise(m,n). \tag{12}$$

The NETD (noise equivalent temperature difference) parameter for the detector (m,n) array is expressed as:

$$NETD(m,n) = \frac{noise(m,n)}{R(m,n)}. \tag{13}$$

The NETD parameter for a detector array is defined as the average NETD of the individual detectors using the relation:

$$NETD_{FPA} = \frac{1}{N_{VN}} \sum_{m=1}^{M} \sum_{n=1}^{N} NETD_{VN}\,(m,n), \tag{14}$$

where:

$$NEDT_{VN}\,(m,n) = \begin{cases} NEDT(m,n) & \text{if} \quad NETD(m,n) < k_{VN}\cdot\overline{NETD} \\ 0 & \text{if} \quad NETD(m,n) \geq k_{VN}\cdot\overline{NETD} \end{cases} \tag{15}$$

$$\overline{NETD} = \frac{1}{MN} \sum_{m=1}^{M} \sum_{n=1}^{N} NETD(m,n), \tag{16}$$

where N_{VN} - number of detectors for which the condition $NETD(m,n) < k_{VN}\cdot\overline{NETD}$, k_{VN} - coefficient selected depending on the type of detector and camera design.

3. Radiometric calibration of a thermal imaging camera

A thermal imaging camera receives not only infrared radiation coming from the observed object, but also radiation coming from elements of the environment (bonfires, people, trees, buildings) and radiation reflected from the surface of the object. Solar radiation also reaches the camera, especially the radiation reflected from the object and the surrounding elements. All radiation components are attenuated by the atmosphere located in the path of radiation propagation. In order to obtain accurate temperature measurement results using a thermal imaging camera, it is necessary to take into account the influence

of various phenomena and radiation sources that interfere with the measurement. Due to the fact that these interferences are difficult to estimate, mathematical models of temperature determination on the basis of registered infrared radiation analysis are simplified in order to achieve required accuracy with possibly the smallest number of analysed parameters. Partial interference compensation can be performed on the basis of such data as: object emissivity, ambient temperature, distance between the object and the camera, relative humidity of the atmosphere. In addition, compensation is often made for the influence on the temperature measurement of such factors as the temperature of the optical elements of the lens (including, for example, the optical windows), the transmission coefficient of the optical elements, the temperature and transmission of the atmosphere and the internal temperature of the camera. It should be noted that when designing a thermal imaging camera, a significant number of physical phenomena must be taken into account, such as: power source noise, detector circuit noise, detector temperature, ambient temperature, digital data processing speed and method, analog-to-digital processing parameters. Taking into account all the phenomena at the highest level is usually impossible or very expensive. Therefore, a compromise solutions between quality and development and production costs are often used, which is most often reflected in camera parameter values.

Radiation from many sources reaches the thermal imaging camera and including all of them (interfering sources) in the temperature determination algorithm is impossible and often pointless. In thermographic equipment, it is most often assumed that infrared radiation from the sources shown in Figure 2 reaches the camera.

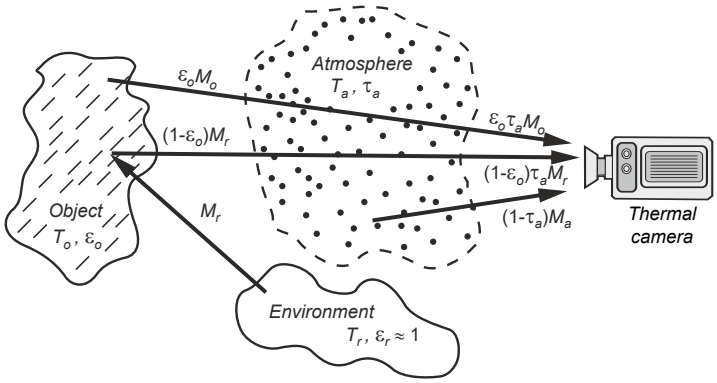

Fig. 2. *Infrared radiation sources in thermographic measurements adopted in the algorithm of temperature determination*

According to the markings in Figure 2, there are three main components of radiation power reaching the camera lens: radiation of the object itself, radiation reflected from the object and radiation of the atmosphere. Then the total radiation power received by the thermal camera from the observed scene (reaching the camera lens) is given by:

$$M_{C\lambda} = \varepsilon_{o\lambda}\tau_{a\lambda}M_\lambda(T_o) + (1-\varepsilon_{o\lambda})\tau_{a\lambda}M_\lambda(T_r) + (1-\tau_{a\lambda})M_\lambda(T_a). \tag{17}$$

where $\varepsilon_{o\lambda}$ is the emissivity of the object, $\tau_{a\lambda}$ is the transmittance of the atmosphere, T_o is the temperature of the object, T_a is the temperature of the atmosphere. The temperature of the other radiation sources is T_r, as the entire environment can be approximated as a blackbody with temperature T_r.

Generally, the radiation reaching the detector of a thermal imaging camera can be divided into the radiation of the served scene ("visible" as radiation of the lens surface L) and radiation of the camera interior - the housing surface H. At the same time, an exchange of energy takes place between the detector and all surfaces surrounding the detector - transfer of energy flux in accordance with the fundamental law of radiometry, according to which the power of radiation emitted by one surface and received by the other surface depends on the distance and relative orientation of two areas in relation to the connecting line [10, 11, 12, 13, 14]. For such assumptions, the power of incident radiation on the detector can be represented by the formulas:

$$\Phi_{L-dD} = A_L F_{L-dD} M_L\left(T_L\right) = A_D F_{dD-L} M_L\left(T_L\right), \tag{18}$$

$$\Phi_{H-dD} = A_H F_{H-dD} M_H\left(T_H\right) = A_D F_{dD-H} M_H\left(T_H\right), \tag{19}$$

$$\Phi_{tot} = \Phi_{L-dD} + \Phi_{H-dD} = A_D F_{dD-L} M_L\left(T_L\right) + A_D F_{dD-H} M_H\left(T_H\right), \tag{20}$$

where: Φ_{X-dD} - - power radiated from the surface X and falling on a discrete detector surface D, F_{X-dD} - view factor (configuration factor) defining what part of the radiation power emitted from the surface X reaches a discrete detector surface D, A_X - area of the surface X, M_X - radiant exitance of surface X, T_X - is the temperature of surface X, X - X represents areas L, H, respectively, A_D is the area of the array detector.

If radiation from an observed scene defined by a radiant exitance $M_{C\lambda}$ falls on a lens and the lens has a transmission $\tau_{L\lambda}$ then:

$$M_L = \tau_{L\lambda} M_{C\lambda}. \tag{21}$$

Additionally, in the adopted camera model, it is assumed that internally the camera surfaces are characterized by an emissivity $\varepsilon_{H\lambda}$. Then the radiant exitance of the housing surfaces is given by the formula:

$$M_H\left(T\right) = \varepsilon_{H\lambda} M_\lambda\left(T_H\right), \tag{22}$$

where $M_\lambda\left(T\right)$ is the spectral distribution of the blackbody radiant exitance as a function of temperature T. From the above formulas and equation (20)), the total power of the radiation incident on the detector can be determined:

$$\Phi_{tot} = A_D F_{dD-L} \cdot \tau_{L\lambda} M_{C\lambda} + A_D F_{dD-H} \cdot \varepsilon_{H\lambda} M_\lambda\left(T_H\right). \tag{23}$$

The power reaching the detector in the analysed model was described by formula (23) taking into account the radiation incident on the detector, which comes from the observed scene and other camera elements. The scene-related radiation component is determined by formula (18) and after taking into account formula (17), the total value of the power of radiation incident on the detector can be expressed as:

$$\Phi_{tot} = A_D F_{dD-L} \cdot \tau_{L\lambda}\left[\varepsilon_{o\lambda}\tau_{a\lambda} M_\lambda(T_o) + (1-\varepsilon_{o\lambda})\tau_{a\lambda} M_\lambda(T_r) + (1-\tau_{a\lambda}) M_\lambda(T_a)\right] + A_D F_{dD-H} \cdot \varepsilon_{H\lambda} M_\lambda\left(T_H\right) \tag{24}$$

Since the infrared detector has a voltage sensitivity $R_v\left(\lambda\right)$ then equation (24) can be written as:

$$\begin{aligned} U_{tot\lambda} \;=\; & A_D F_{dD-L}\tau_{L\lambda}\varepsilon_{o\lambda}\tau_{a\lambda} R_{v\lambda} M_\lambda(T_o) + A_D F_{dD-L}\tau_{L\lambda}(1-\varepsilon_{o\lambda})\tau_{a\lambda} R_{v\lambda} M_\lambda(T_r) + \\ & A_D F_{dD-L}\tau_{L\lambda}(1-\tau_{a\lambda}) R_{v\lambda} M_\lambda(T_a) + A_D F_{dD-H} \cdot \varepsilon_{H\lambda} R_{v\lambda} M_\lambda\left(T_H\right), \end{aligned} \tag{25}$$

The infrared detector array receives radiation in the spectral band $\lambda \in \langle\lambda_1, \lambda_2\rangle$ and if we assume that for this wavelength range the emissivity and transmission values are not wavelength dependent, then $\varepsilon_{o\lambda} = \varepsilon_o = const,\ \varepsilon_{H\lambda} = \varepsilon_H = const,\ \tau_{a\lambda} = \tau_a = const,\ \tau_{L\lambda} = \tau_L = const.$ As a result the equation (25) can be written in the following form:

$$\begin{aligned} U_{tot} \;=\; & A_D F_{dD-L} \cdot \tau_L \varepsilon_o \tau_a \int_{\lambda_1}^{\lambda_2} R_{v\lambda} M_\lambda(T_o) d\lambda + A_D F_{dD-L} \cdot \tau_L (1-\varepsilon_o)\tau_a \int_{\lambda_1}^{\lambda_2} R_{v\lambda} M_\lambda(T_r) d\lambda + \\ & A_D F_{dD-L} \cdot \tau_L (1-\tau_a) \int_{\lambda_1}^{\lambda_2} R_{v\lambda} M_\lambda(T_a) d\lambda + A_D F_{dD-H} \cdot \varepsilon_H \int_{\lambda_1}^{\lambda_2} R_{v\lambda} M_\lambda\left(T_H\right) d\lambda, \end{aligned} \tag{26}$$

Assuming determination:

$$U_D(T) = \int_{\lambda_1}^{\lambda_2} R_{v\lambda} M_\lambda\left(T\right) d\lambda. \tag{27}$$

we obtain that the total voltage on the detector resulting from the incident radiation is:

$$\begin{aligned} U_{tot} \;=\; & A_D F_{dD-L} \cdot \tau_L \varepsilon_o \tau_a U_D(T_o) + A_D F_{dD-L} \cdot \tau_L (1-\varepsilon_o)\tau_a U_D(T_r) + \\ & A_D F_{dD-L} \cdot \tau_L (1-\tau_a) U_D(T_a) + A_D F_{dD-H} \cdot \varepsilon_H U_D\left(T_H\right). \end{aligned} \tag{28}$$

An approximation function can be used to determine the detector voltage U_D as a function of temperature T of the observed objects for the given spectral range [15]:

$$U_D(T) = \frac{R}{e^{\frac{B}{T}} - F} + O \tag{29}$$

where R, B, F, O are constants determined at the camera calibration stage. The R constant is used to adjust the response of the system. The B constant is determined to take into account the spectral properties for the effective wavelength. Nonlinearities are taken into account by means of F constant. The O constant (offset) makes it possible to take into account the operating point of the system. For the above assumptions, equation (28) can be written in the following form:

$$\begin{aligned} U_{tot} \;=\; & A_D F_{dD-L} \cdot \tau_L \varepsilon_o \left(\frac{R}{e^{\frac{B}{T_o}} - F} + O\right) + A_D F_{dD-L} \cdot \tau_L (1-\varepsilon_o) \left(\frac{R}{e^{\frac{B}{T_r}} - F} + O\right) + \\ & A_D F_{dD-L} \cdot \tau_L (1-\tau_a) \left(\frac{R}{e^{\frac{B}{T_a}} - F} + O\right) + A_D F_{dD-H} \cdot \varepsilon_H \left(\frac{R}{e^{\frac{B}{T_H}} - F} + O\right). \end{aligned} \tag{30}$$

To determine the temperature of the observed object, equation (30) should be transformed to the form:

$$T_o = B \left\{ \ln \left[\frac{R}{\frac{U_{tot} - A_D \cdot \tau_L (1-\varepsilon_o) U_D(T_r) - A_D F_{dD-L} \cdot \tau_L (1-\tau_a) U_D(T_a) - A_D F_H \cdot \varepsilon_H U_D(T_H)}{A_D F_{dD-L} \cdot \tau_L \varepsilon_o} - O} + F \right] \right\}^{-1} \tag{31}$$

Measuring the temperature of an object using equation (31) requires knowledge of the values of the R, B, F and O parameters of the approximation function (30). To determine the values of these parameters, one must measure the values of the detector voltage U_{tot} for different values of temperatures T_o i T_H. The calculations required to determine the R, B, F and O parameters by the method of least squares were performed using digital data processing.

4. Test site design

In order to determine the quality of a tested thermal imaging camera, many camera parameters such as sensitivity, non-homogeneity, NETD, MRTD, non-uniformity correction (NUC) and radiometric calibration must be measured and determined. In order to carry out research, testing, objective evaluation and comparison of thermal imaging cameras, it is necessary to have a suitable laboratory and research base for measuring and controlling parameters and analysis of characteristics and relationships. Therefore, a special automated measuring station was developed to determine the parameters and calibration of the tested thermal imaging camera. The stand consists of such basic elements as: a set of blackbodies with adjustable temperatures, a table with a cart, a table controller, a climate chamber, an IR Capture data capturing device, software for data analysis and processing and a computer with control software. A block diagram of the data acquisition and parameter determination station for the thermal imaging camera is shown in Figure 3 .

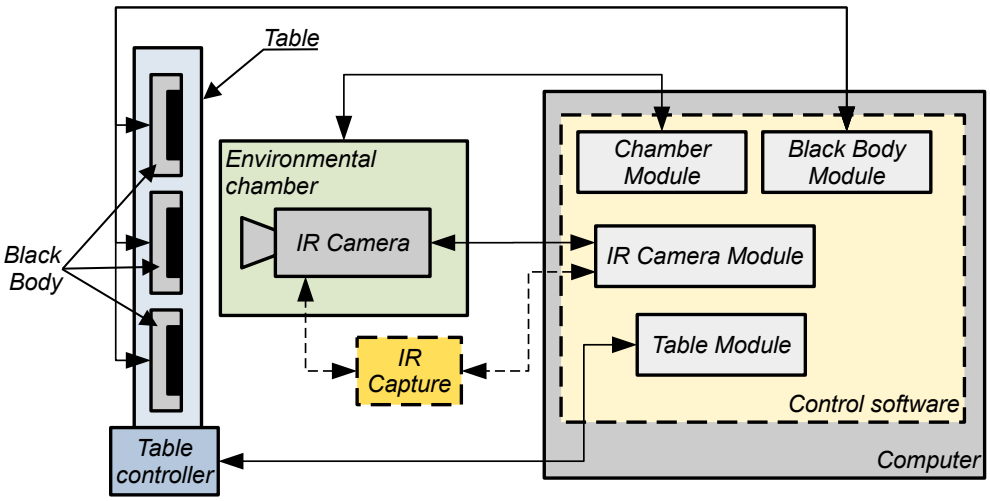

Fig. 3. *Schematic of the station for data recording and determination of thermal camera parameters*

An essential component of a thermal imaging camera performance measurement workstation is the control software. Thermographic data from a thermal camera can be recorded by the control software in two ways. The primary method of data transmission is via the Ethernet interface. With this interface, data can be transmitted to a computer without any additional hardware. If the thermal imaging camera is equipped with another communication interface, in particular if it is not present on a typical PC, the IR Capture device can be used as an option. The thermal camera transmits image data to the IR Capture device via its own communication bus, e.g. VideoBus [5]. A PC then receives the data from IR Capture via the Ethernet bus. In addition, the PC is used to set the parameters of the blackbody, to control the table for the positioning of blackbodies and to control the climate chamber.

One of the most important factors influencing the performance of a thermal imaging camera is the ambient temperature. In order to analyse the measured and determined parameters of the thermal imaging camera as a function of the ambient temperature, the automated test stand was equipped with the SH-661 climatic chamber from ESPEC. The basic parameters of the chamber are presented in Table 1, while Figure 4a shows a photograph of the climatic chamber with a microbolometer thermal imaging camera inside.

An essential component of a thermal imaging camera testbed are extended area blackbodies. The task of blackbodies is to generate infrared radiation that uniformly illuminates the focal plane array of the thermal imaging camera under test. At the same time, the flux of the generated radiation is dependent on the temperature of the blackbody. Therefore, a blackbody

Table 1. *Basic parameters of the SH-661 climatic chamber by ESPEC*

Parameter	Value
Temperature range	-60°C ÷ +150°°C
Humidity control	30 to 95% rh
Internal dimensions (HxWxD)	400 x 400 x 400 mm
Interface for communication with a computer	RS485 serial port

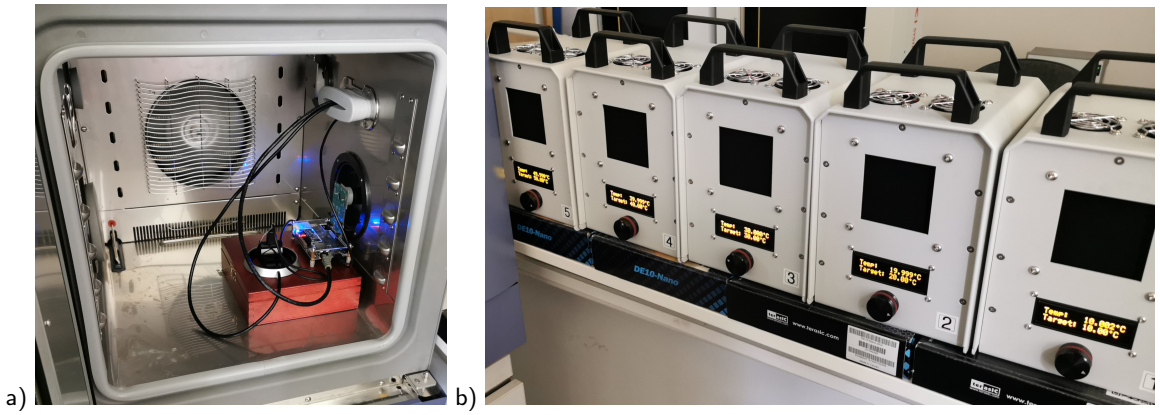

a) b)

Fig. 4. *View of a thermal imaging camera inside the climatic chamber (a) and a set of technical blackbodies with embedded controllers developed at the Institute of Optoelectronics WAT (b)*

must have a high emissivity coefficient and very good temperature stability. Additionally, due to the accuracy of the parameters determined, the temperature difference between black bodies should be greater than 10°C. Selected blackbody parameters are listed in Table 2 .

Table 2. *Basic parameters of extended area blackbody developed and manufactured in IOE WAT*

Parameter	Value
Black body area	62 mm x 62 mm
Absolute temperature range	10°C ÷ 60°C (for ambient temp. 20°C)
Average directional emmisivity at 20°angle	0.985
Average directional emmisivity at 60°angle	0.973
Average hemispheric emmisivity	0,944
Temperature accuracy	0.01°C

The bench is equipped with a set of 5 blackbodies developed and manufactured in the Institute of Optoelectronics, MUT (Fig. 4b). The blackbodies were mounted on a linearly moving table with a programmable controller. This solution allows for an automated change of a blackbody observed by a thermal imaging camera. The table is controlled by the control software via RS-232 or MODBUS-RTU communication interface.

A table with a programmable controller was used to automatically change the blackbody observed by the thermal imaging camera. The table provides linear travel and its construction is based on an aluminium profile, a linear guide and a carriage, which ensures precise and repeatable positioning. The stepper motor is controlled by a built-in controller, which can move the carriage to any position within its travel range. The controller communicates with the control software via the RS-232 or MODBUS-RTU interface.

5. Summary

As a result of data registration performed at the test stand, it was possible to determine the values of many parameters of both the focal plane array detector and the entire camera, as well as to perform calibration of the thermal imaging camera in terms of remote temperature measurement. A great advantage of the test stand on is the considerable level of automation of measurements and determination of parameters. Automation was achieved mainly through the use of proprietary software for control and calculation of parameter values. This allows for multiple repetition of measurements with high reliability and

reduction of the impact of human errors. The use of multiple blackbodies and a climatic chamber allows for simulating the conditions of the observed scene and environmental conditions, in particular ambient temperature and humidity. This allows for quality assessment and comparison of tested thermal imaging cameras in terms of many parameters. An exemplary result of the measurements carried out using the developed test stand is shown in Figure 5. The figure presents a plot of voltage of a single microbolometer from array detector recorded with the ADC converter as a function of the climate chamber temperature. The data were recorded while observing black bodies with different temperatures.

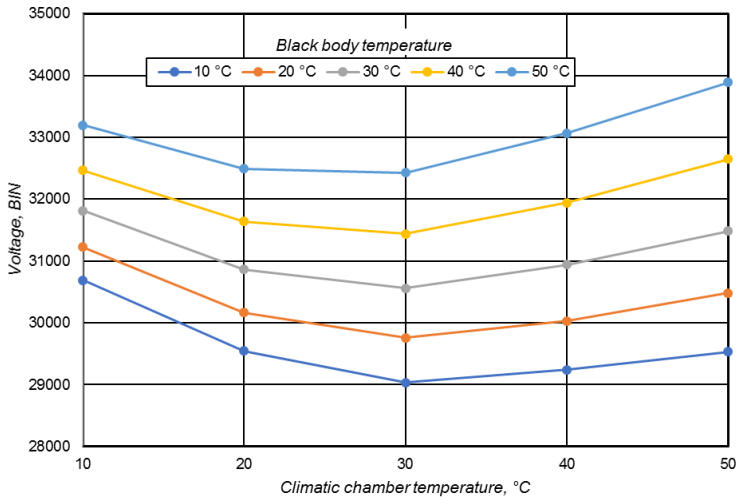

Fig. 5. *Plot of microbolometer detector voltage as a function of climate chamber temperature for black bodies at different temperatures*

The developed model for the measurement-based calibration of a thermal imaging camera taking into account ambient temperature changes and blackbody-based measurement correction was tested during a test measurement session. Data from the session were used to determine the R, B, F and O coefficients of the formula approximating the camera model performance. In addition, a scene recording was performed with objects whose temperature was measured in the presence of blackbodies as reference sources. The measurement layouts are shown in Figures 6a and 6b. The measurement areas are marked with a yellow rectangle, while the red and blue colors indicate the areas constituting reference sources at 45°C and 35°C, respectively. Temperature was measured at two measurement points I (center of yellow square, coordinates 320×140 – Fig. 6a) and II (center of yellow square, coordinates 450×140 square – Fig. 6b). The obtained temperature measurement results are shown in Figures 7a and 7b. For the temperature measured at each point, the experimental standard deviation (Figures 8a and 8a) and the expanded uncertainty with a confidence level of 99 % were calculated (Figures 9a and 9a).

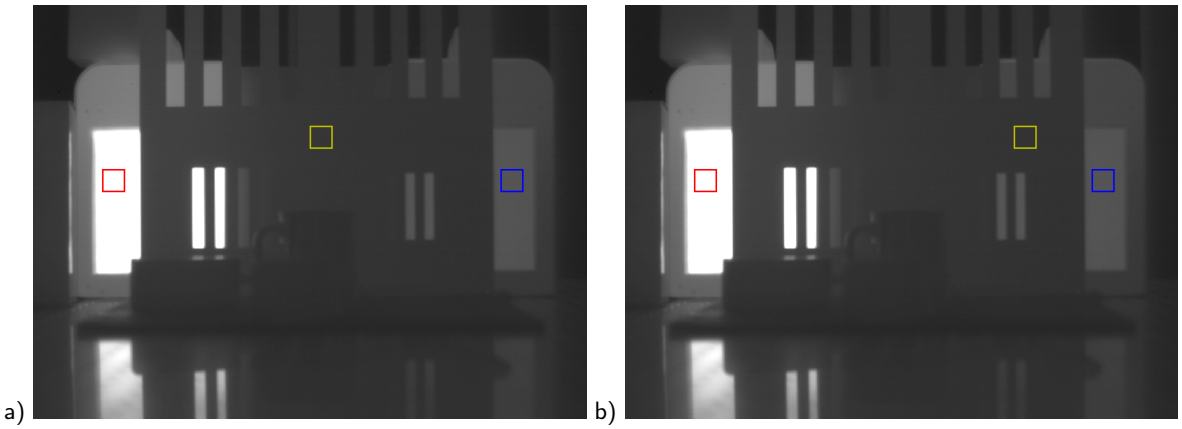

Fig. 6. *View of the scene with measurement areas marked - point I (a), point II (b)*

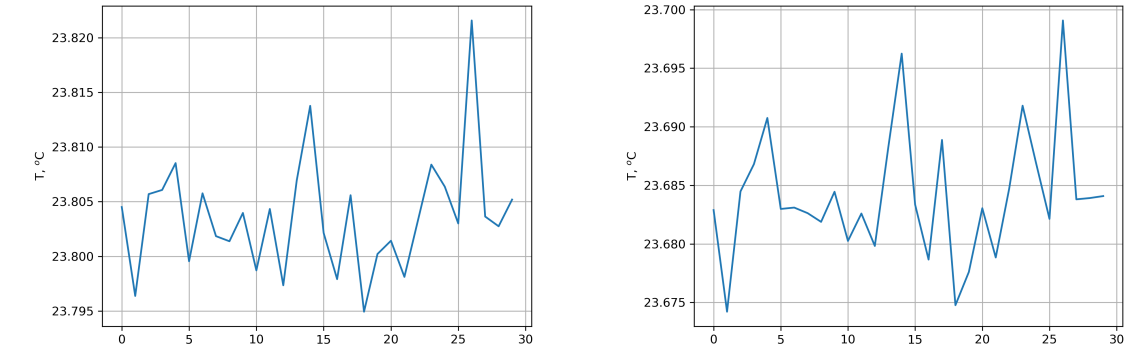

a) b)

Fig. 7. *Diagram of temperature measured in measuring point I (a) and II (b)*

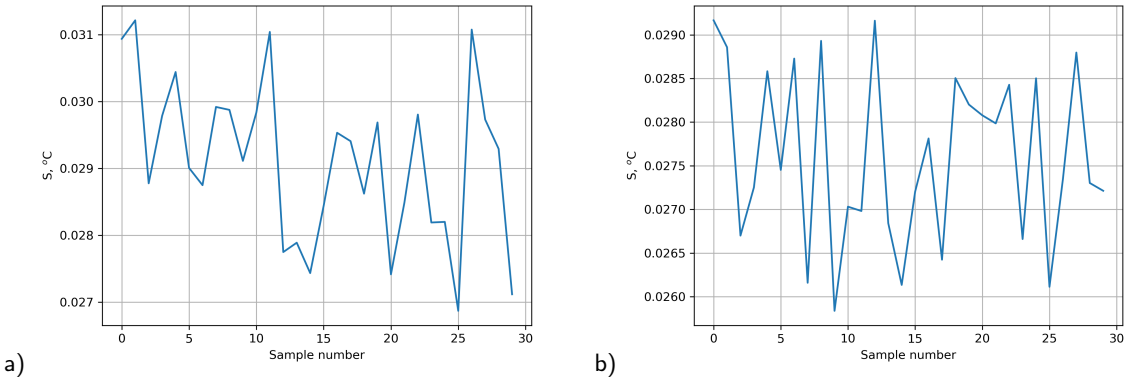

a) b)

Fig. 8. *Experimental standard deviation for measured temperature as a function of measurement no. (image frames) for point I (a) and II (b)*

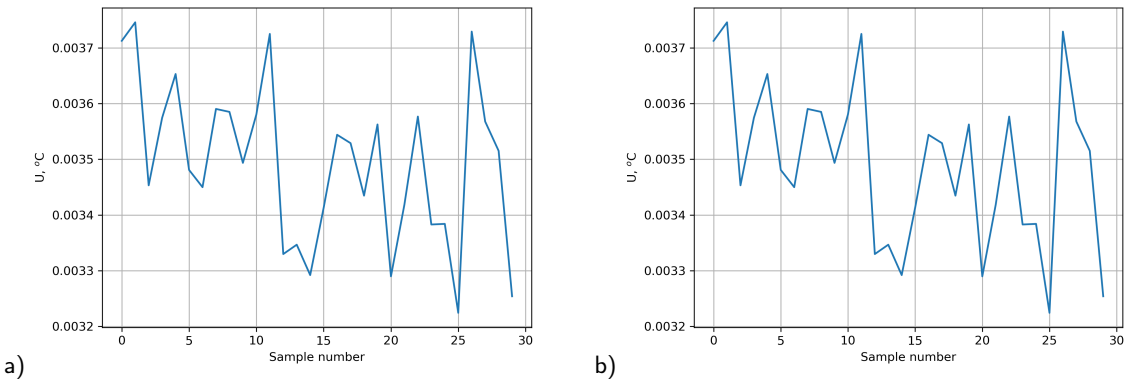

a) b)

Fig. 9. *Expanded uncertainty with a confidence level of 99 % for measured temperature as a function of measurement no.*

Acknowledgments

The research was co-financed by the National Center for Research and Development as the part of the project "FACE-COV ™ - a system solution for automatic monitoring of public places by the thermal imaging method and detection of

SARS-COV2 infection markers using artificial intelligence with the option of biometric identification (digital tagging) meeting the standards of medical devices" grant no. POIR.01.01.01-00-0662/20, through the European Regional Development Fund under the European Union Smart Growth Programme.

References

[1] Tomasz Sosnowski, Henryk Madura, Grzegorz Bieszczad, Mariusz Kastek, and Krzysztof Chmielewski. Construction, parameters, and research results of thermal weapon sight. In *Proceedings of SPIE - The International Society for Optical Engineering*, volume 8193, 2011.

[2] Grzegorz Bieszczad, Michał Krupiński, Henryk Madura, and Tomasz Sosnowski. Thermal camera for autonomous mobile platforms. In Aleksander Nawrat and Zygmunt Kuś, editors, *Vision Based Systemsfor UAV Applications*, pages 95–114. Springer International Publishing, 2013.

[3] T. Sosnowski, G. Bieszczad, H. Madura, and M. Kastek. Thermovision system for flying objects detection. In *Thermovision system for flying objects detection*, pages 141–144, 2018.

[4] David L Perry and Eustace L Dereniak. Linear theory of nonuniformity correction in infrared staring sensors. *Optical Engineering*, 32(8):1854–1859, 1993. Publisher: SPIE.

[5] Tomasz Sosnowski, Grzegorz Bieszczad, Mariusz Kastek, and Henryk Madura. Digital image processing in high resolution infrared camera with use of programmable logic device. In *Proceedings of SPIE - The International Society for Optical Engineering*, volume 7838, 2010.

[6] Grzegorz Bieszczad, Tomasz Sosnowski, Henryk Madura, Mariusz Kastek, and Jarosław Bareła. Adaptable infrared image processing module implemented in FPGA. In *Proceedings of SPIE - The International Society for Optical Engineering*, volume 7660, 2010.

[7] Grzegorz Bieszczad, Sławomir Gogler, Tomasz Sosnowski, Henryk Madura, Juliusz Kucharz, and Alicja Zarzycka. Determining the responsivity of microbolometer FPA using variable optical aperture stop. In *Proceedings of SPIE - The International Society for Optical Engineering*, volume 8541, 2012.

[8] Paul W. Kruse. *Uncooled Thermal Imaging Arrays, Systems, and Applications*. SPIE, 1000 20th Street, Bellingham, WA 98227-0010 USA, 2001.

[9] Jean-Luc Tissot, Frederic Rothan, Corrinne Vedel, Michel Vilain, and Jean-Jacques Yon. LETI/LIR's uncooled microbolometer development. In Bjorn F. Andresen and Marija Strojnik, editors, *Infrared Technology and Applications XXIV*, volume 3436, pages 605 – 610. International Society for Optics and Photonics, SPIE, 1998.

[10] Bogusław Więcek and Gilbert De Mey. *Termowizja w podczerwieni. Podstawy i zastosowania*. Wydawnictwo PAK, 2011.

[11] Cornelius J. Willers. *Electro-Optical System Analysis and Design: A Radiometry Perspective*. SPIE, 2013.

[12] William L. Wolfe. *Introduction to radiometry*. SPIE Press, 1998. Pages: 200.

[13] Michael Vollmer and Klaus Peter Möllmann. *Infrared thermal imaging: Fundamentals, research and applications*. Wiley Blackwell, 2017.

[14] John R. Howell, M. Pinar Mengüç, and Robert Siegel. *Thermal Radiation Heat Transfer*. CRC Press, 6 edition edition, 2015.

[15] Nicolas Horny. FPA camera standardisation. *Infrared Physics and Technology*, 44(2):109–119, 2003.